PHYSICAL REVIEW B **103**, 094406 (2021)

Magnetoelectric effect in a single crystal of the frustrated spinel $CoAl_2O_4$

Chandan De,[1,2,3] Rabindranath Bag,[4] Surjeet Singh,[4] Oscar Fabelo ,[5] Maria Teresa Fernández-Díaz,[5]
N. V. Ter-Oganessian ,[6] and A. Sundaresan [1,*]
[1] *School of Advanced Materials, Chemistry and Physics of Materials Unit, Jawaharlal Nehru Centre for Advanced Scientific Research, Jakkur P.O., Bangalore 560064, India*
[2] *Laboratory for Pohang Emergent Materials, Pohang Accelerator Laboratory, Pohang 37673, Republic of Korea*
[3] *Center for Artificial Low Dimensional Electronic Systems, Institute for Basic Science (IBS), Pohang 37673, Republic of Korea*
[4] *Indian Institute of Science Education and Research, Pune 411008, India*
[5] *Institut Laue-Langevin, 71, Avenue des Martyrs, CS 20156, 38042 Grenoble Cedex 9, France*
[6] *Institute of Physics, Southern Federal University, Rostov-on-Don 344090, Russia*

(Received 23 November 2020; revised 10 February 2021; accepted 18 February 2021; published 4 March 2021)

The magnetic ground state of $CoAl_2O_4$ has been a controversial issue because the ratio of nearest- (J_1) to next-nearest-neighbor (J_2) exchange interactions in the diamond lattice is close to the boundary between a spiral spin liquid and a long-range ordered antiferromagnetic ground state. Recently, Ghara *et al.* reported a linear magnetoelectric effect in a polycrystalline $CoAl_2O_4$ and attributed it to a long-range magnetic order. However, the magnetic ground state and the easy axis anisotropy remained unsolved. Here we propose the easy magnetic axis direction by comparing the results of magnetoelectric measurements in a high-quality single crystal with phenomenological calculations. From the value of polarization ratio $P||[1\text{-}10]$ measured under magnetic field applied along $H||[1\text{-}10]$ and $H||[001]$, we determined that the magnetic easy axis is along [111]. The single ion contribution of the magnetic ions located at the noncentrosymmetric environment is responsible for the magnetoelectric effect similar to that observed in other *A*-site magnetic spinel oxides, Co_3O_4, MnB_2O_4 ($B =$ Al, Ga).

DOI: 10.1103/PhysRevB.103.094406

I. INTRODUCTION

The frustrated spin systems have come to the current research frontiers because of their exotic physical states such as spin-glass, spin-liquid, spin-ice, a cluster of spins, and heavy fermion-like behavior of spins [1–7]. The spinel system with the chemical formula AB_2X_4 is one of the most conversant magnetic compounds where both *A* and *B* are metal cations, magnetic or nonmagnetic, and *X* is an anion [8–13]. In this chemical unit cell, the BO_6 octahedra connected by edge-sharing form a pyrochlore lattice structure, causing a geometrical frustration. On the other hand, the *A* site forms a diamond structure consisting of two interpenetrated face-centered cubic lattices, where the intriguing magnetic interactions and their consequences are highly diverse [1]. In 1964, a systematic study of spinel systems with $A = Co^{2+}$, Mn^{2+}, and Fe^{2+}, and $B = Al^{3+}$, Co^{3+} reported magnetic order of the *A*-site spins in the presence of different *B*-site nonmagnetic ions [8]. It revealed a magnetic frustration at the *A* site, depending on the magnetic ions and the nonmagnetic ions at the *B* site. For example, Mn^{2+} shows a long-range antiferromagnetic (AFM) ordering, Co^{2+} shows a very weak magnetic correlation at low temperatures, while Fe^{2+} shows no long-range ordering even below mK temperature when Al^{3+} ions occupy the *B* site in all the compounds [14]. Recently, a dynamic spin fluctuation was observed in $CuAl_2O_4$ [15]. On the other hand, Co^{2+} ions undergo a long-range ordering above 30 K in Co_3O_4, where the Co^{3+} ions occupying the *B* site are nonmagnetic [8,16]. This was explained based on the exchange path *A*-*X*-*B*-*X*-*A* in the diamond lattice, where two AFM interactions, namely, nearest neighbor J_1 (between the two FCC lattices) and next-nearest neighbor J_2 (in one FCC lattice between the corner and the face center), are significant (Fig. 1).

Considering this model of two exchange constants, Bergman *et al.* have theoretically proposed a highly degenerate set of classical coplanar spiral-spin-liquid states for $J_2/J_1 > 1/8$, whose propagation wave vectors form a continuous surface in momentum space [1]. This model also explains the long-range AFM ordering in $MnAl_2O_4$ and Co_3O_4, where the ratio J_2/J_1 is less than 1/8. On the other hand, $MnSc_2S_4$ with $J_2/J_1 \sim 0.85$ shows a spiral spin liquid state. However, for $CoAl_2O_4$, J_2/J_1 is very close to 1/8; hence the ground state magnetism becomes ambiguous, whether it is a long-range AFM ordering, spiral-spin-liquid state, or a spin-glass state [17–21]. Apart from the frustrating magnetic interactions, another crucial factor in $CoAl_2O_4$ is the cation inversion ratio [18]. The cation inversion among the Co^{2+} and Al^{3+} ions seems to be unavoidable up to a specific limit, thus making this system even more complicated. The degree of inversion parameter can be defined by *x* in the formula $[Co_{1-x}Al_x][Al_{2-x}Co_x]O_4$ where the value of *x* mainly depends on the sample preparation conditions [19]. Considering a minimal inversion parameter, this A-site frustrated

---

[*] sundaresan@jncasr.ac.in

magnetic spinel $CoAl_2O_4$ was demonstrated to realize a spiral-spin-liquid ground state [18]. A piece of evidence came from a single crystal neutron scattering experiment, which showed an unconventional magnetic state below a magnetic transition temperature ∼8 K [21]. The magnetic Bragg peaks were broad, and their line shape had a Lorentzian contribution. Thus, the observed short-range magnetic correlations were explained by the spiral-spin-liquid model [18]. Further, by the same authors, an unconventional magnetic state had been attributed in $CoAl_2O_4$ again using a single crystal study. It raised another intriguing fact that the microstructure, particularly [111] twin boundaries, also could be responsible for the unusual magnetism in addition to the next-nearest-neighbor interaction for the frustration [21]. The arguments became more intriguing when another group, based on single-crystal neutron scattering, classified $CoAl_2O_4$ as a kinetically inhibited antiferromagnet where the long-range correlation of magnetic ground states would be blocked by the freezing of domain-wall motion below an unusual magnetic phase transition at $T^* = 6.5\,\mathrm{K}$ [22]. This proposal was further supported by another single crystal study, which showed an unchanged spin correlation between $T = 2\,\mathrm{K}$ and 250 mK, and that was consistent with the frozen magnetic ground state. An inhomogeneous and slow magnetic fluctuation and short-range magnetic correlations were revealed by local spin probes such as nuclear magnetic resonance, electron spin resonance, and muon spin relaxation studies [23]. In fact, with the comparative study on the spinel $MnAl_2O_4$, which had a clear AFM phase transition below 39 K despite being prone to the cation inversion, the authors showed that $CoAl_2O_4$ is a unique case where the effect of next-nearest-neighbor exchange interaction has a primary effect rather than the cation inversion [24]. Further support to the spiral-spin-liquid state comes from the study of varying the cation inversion with different heat treatments of the sample [19]. For higher cation inversions $x \geqslant 0.101$, a spin-glass state has been reported [19,25]. Concurrently, Roy *et al.* had reported a long-range correlation at low temperature for the minimum cation inversion sample by nuclear magnetic resonance and neutron diffraction studies, which led them to propose an easy magnetic axis along the [100] direction [20]. Ghara *et al.* have recently reported the long-range antiferromagnetically ordered ground state from a magnetoelectric study in a polycrystalline material with the minimum site inversion parameter of $x \sim 0.05$ [26]. However, the actual magnetic ground state and the magnetic easy axis determination still have to be derived from a single crystal study with the caution of site inversion parameter in the growth process, which would be challenging.

Therefore, to elucidate the above scenario, we have grown the high-quality single crystal of $CoAl_2O_4$ using the floating zone technique with particular attention to the cation disorder. We have examined the dielectric and pyroelectric properties along different crystallographic directions and confirm the long-range magnetic ordering and magnetoelectric effect in the high-quality $CoAl_2O_4$ single crystal with low inversion. From a comparison of polarization values observed under magnetic fields applied at different directions with phenomenological calculations, we propose the easy axis to be along [111]. The neutron Laue diffraction also supports our study.

II. EXPERIMENTS

Polycrystalline samples of $CoAl_2O_4$, prepared via conventional solid-state route using Al_2O_3 and Co_3O_4 with 0, 5, 10, and 15% excess of Co_3O_4, were used for single crystal growth using a floating zone furnace. The powder synthesis was performed at 1000 °C for 12 h and 1100 °C for 24 h. Finally, the sample was heated at 1100 °C for 24 h and cooled to room temperature with 0.5 °C/min. Nearly 8-cm rods were made from the synthesized powder using hydrostatic pressure for the different excess of Co_3O_4 and sintered at 1150 °C for 24 h and cooled to room temperature with 0.5 °C/min rate. The crystals were grown using a four-mirror type infrared image furnace (Crystal System Corporation FZ-T-10000-H-III-VPR) equipped with four 1-kW halogen lamps with the following growth conditions. For the individual excess Co_3O_4 containing sintered rod, the growth speed was varied from 1 to 6 mm/h to obtain the possible lowest disordered crystal. The feed and seed rods were kept spinning at 20 rpm in opposite directions for all the crystal growth experiments. Motivated by the previous crystal growth procedure in this sample, a mixture of Ar and O_2 gas flow with 95:5 ratios were used in all cases [27]. Nearly 5-cm-long crystals were obtained from each growth experiment of different excess Co_3O_4 containing samples. Crystal homogeneity was confirmed by optical microscopy under polarized light and scanning electron microscopy (Zeiss Ultra Plus, Germany). The lowest disordered sample was found with a 10% excess of Co_3O_4.

Further, the crystal with 10% excess was annealed at 1050 °C for two days and finally cooled to room temperature with 6 °C/h rate. The crystal boule was cut into a cubic shape along the [001] and [110] planes with a dimension of about 2 mm × 2 mm × 2 mm, used for magnetic measurements. For dielectric and pyroelectric measurements, the samples were further cut into thin square plates with a dimension of 2 mm × 2 mm × 0.5 mm along with the three orthogonal directions [001], [110], and [1–10] while keeping the other orthogonal direction as arms of the sample for the application of the magnetic field. Electrodes were made on the wide surface applying silver paste (PELCO High-Performance Silver Paste). Finally, dielectric measurements were carried out using Agilent E4980A Precision LCR meter, and the pyroelectric current was recorded using Keithley Electrometer (6517A) in a Physical Property Measurement System (PPMS). Heat capacity was measured in PPMS by the thermal-relaxation calorimeter. Magnetic measurements were performed in a superconducting quantum interference device magnetometer (Quantum Design MPMS-4).

III. RESULTS AND DISCUSSIONS

A. Structural data

X-ray diffraction data collected on crushed powders at room temperature confirmed a single-phase Fd-3 m structure. The lattice parameter obtained from the Rietveld refinement is 8.10 Å, which is very close to the previously reported value (Fig. 2). Further, our refinement also shows the Co^{2+} and

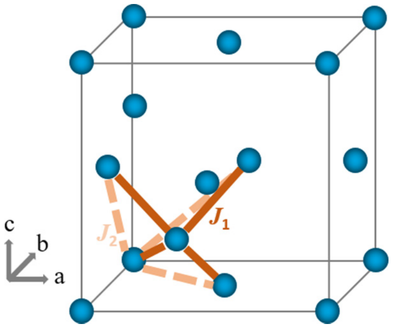

FIG. 1. Diamond lattice comprised of Co^{2+} ions in $CoAl_2O_4$. Dark brown solid lines represent the nearest-neighbor (J_1), and light brown dashed lines represent next-nearest-neighbor (J_2) exchange interactions.

Al^{3+} site inversion of nearly 5% [28], which agrees with the recent report in the polycrystalline sample [26]. An as-grown crystal boule with ∼5.5-mm diameter and over 2 cm in length is shown in Fig. 2(d). The Laue diffraction spots for [110] and [001] directions [Figs. 2(b)–2(c)], and a cubic geometry cut specimen with the [110], [1–10], and [001] orthogonal direction is shown in Fig. 2(d). This cubic specimen was used for the magnetic measurements, and the plate-shaped samples, obtained by cutting it further as described above, were used for the electrical measurements. The schematic Fig. 2(e) shows the various orthogonal directions in the cubic crystal.

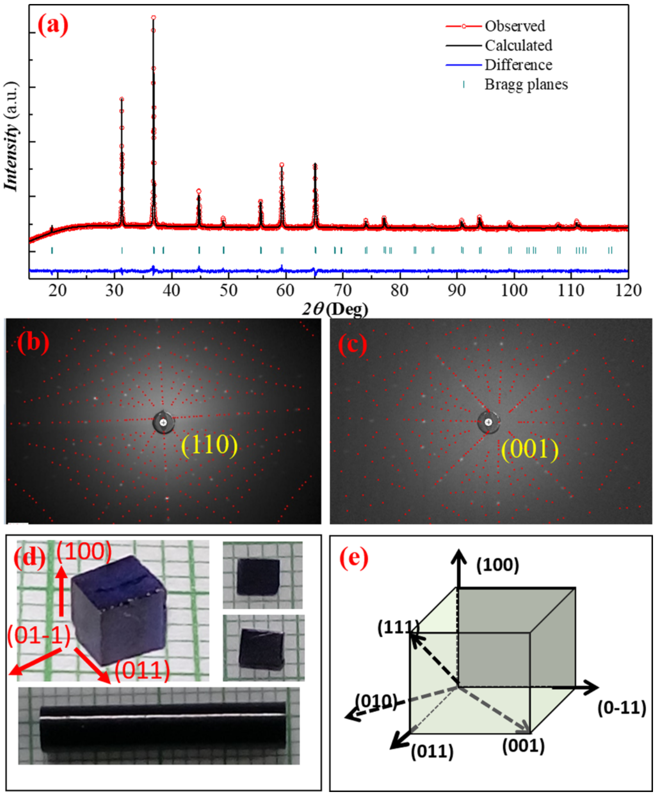

FIG. 2. (a) Rietveld refinement of powder x-ray diffraction pattern at room temperature of $CoAl_2O_4$ obtained from the crushed crystal. The red circles, black lines, blue lines, and aqua vertical lines represent the experimental data, simulated data, and residue and Bragg planes. (b), (c) Laue diffracted spots overlapping with the simulated spots along the [110] and along the [001] direction. (d) As-grown crystal boule in the bottom image, cubic shape cut crystal along the [100], [01-1], and [011] directions (Top left), thin plate square shape cut crystal pieces for magnetic and electrical measurements (right). (e) Schematic diagram to visualize the crystal directions.

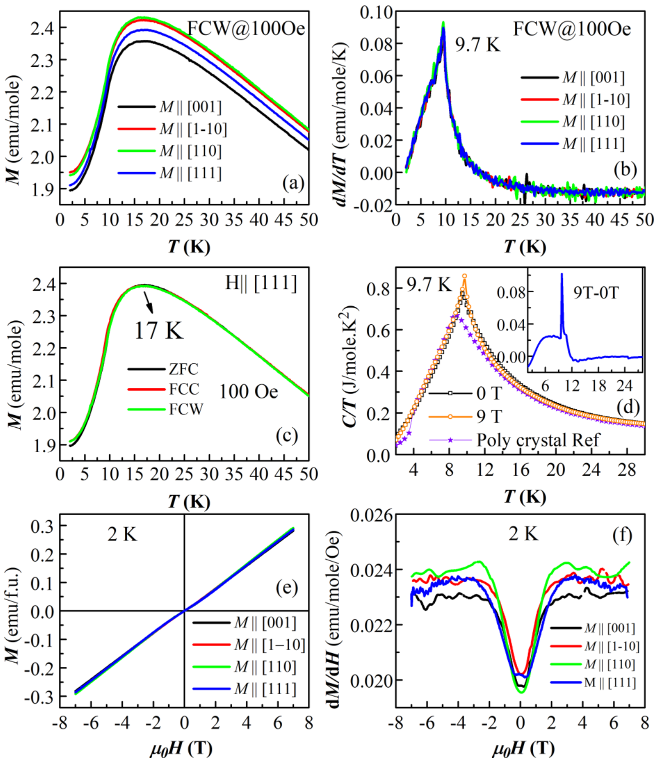

FIG. 3. (a) DC magnetization measured along various crystallographic directions of $CoAl_2O_4$ with cubic shape. Black, red, green, and blue curves represents moments along [001], [1–10], [110], [111], respectively. (b) The corresponding first derivative of magnetization with temperature. (c) DC magnetization measured under ZFC, FCC, and FCW condition along the [111] direction. (d) Heat capacity (Cp/T) as a function of temperature under zero field (black) and 9 T (orange) magnetic field. Inset shows the difference value of Cp ($H = 9\,\mathrm{T}$) and Cp ($H = 0\,\mathrm{T}$). Star symbol curve showing polycrystalline data taken from Ref. [26] for comparison. (e) $M(H)$ loop recorded at 2 K, along the [001], [1–10], [110], and [111] directions. (f) The corresponding first derivative of magnetization (dM/dH) with the field.

B. Magnetization and heat capacity

Figure 3 shows the magnetization data measured along various crystallographic directions of [110], [1–10], [001], and [111] under field–cooled warming (FCW) condition with 100 Oe. We can see a broad peak centered at 17 K and a sharp decreasing trend below 10 K. This magnetization anomaly is quite similar to what was observed in an earlier study for a sample with a minimum site inversion parameter [26]. This magnetization peak does not look like a typical AFM feature, and it is not possible to distinguish the spiral-spin-liquid state or the long-range magnetic ordering state in this sample. We have taken the first derivative of magnetization with respect to

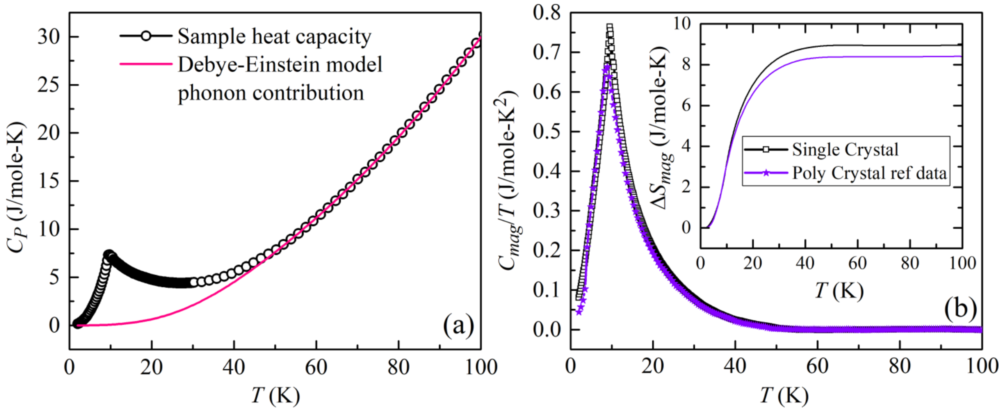

FIG. 4. (a) Sample heat capacity versus temperature curve and the fitted phonon contributions from the Debye-Einstein model. (b) Extracted magnetic contribution of heat capacity ($C_{\rm mag}/T$) with temperature for our single crystal along with adopted polycrystalline reference data. The inset shows the entropy change associated with the magnetic contribution of the heat capacity both from our single crystal and adopted polycrystalline data. The violet star symbol curve represents the polycrystalline data adapted from Ref. [26] for comparison.

temperature, which shows a rather sharp peak close to 10 K independent of crystallographic axes [Fig. 3(b)]. Further, we have measured magnetization with zero-field (ZFC) and field cooled cooling (FCC) conditions to see if there is any splitting, which would indicate a spin-glass-like behavior. We can see that the ZFC, FCC, and FCW magnetization curves overlap quite well, almost down to low temperatures. As discussed in the introduction, the magnetic property in $\mathrm{CoAl_2O_4}$ is susceptible to the amount of the cation inversion between the A and B sites. Sample with an inversion factor ($x \geqslant 0.08$) has been shown to have spin-glass behavior, whereas ($0.05 \leqslant x \leqslant 0.08$) has been anticipated to have a spin liquid ground state [14,17,19].

The absence of splitting of the ZFC and FCW data suggests that the sample may have a long-range ordering. The $1/\chi_m$ vs T data measured under the FCW condition under 100 Oe were fitted with Curie-Weiss law in the temperature range of 50 to 300 K [28]. The obtained effective moment (4.87 μ_B) is higher than the theoretical spin only moment (3.87 μ_B) value, suggesting a significant orbital moment for the $\mathrm{Co^{2+}}$ ions. On the other hand, the obtained Curie-Weiss temperature (θ_{CW}) is close to -88 K. The value of $|\theta_{CW}|$ is much higher than the likely long-range ordering temperature ($\sim$10 K). Therefore, the estimated frustration parameter ($|\theta_{CW}|/T_N \sim 9$) suggests a significant strength of the next-nearest-neighbor interaction (J_2), yielding a high magnetic frustration. Figure 3(e) shows the magnetic field dependence of magnetization measured at 2 K in various directions. $M(H)$ curves overall behavior is linear for all the directions except a small change in the slope around 2 T. To get more insight, we have taken the first derivative of magnetization with respect to the field and shown in Fig. 3(f). The slope change is evident in the dM/dH curve at 2 T.

Figure 3(d) shows C_p/T versus temperature data measured at zero fields and 9 T magnetic field. The Cp/T curves show a sharp peak at 9.8 K, which further suggests a long-range magnetic ordering occurring below this temperature. Further, this heat capacity data can be compared with the previously reported by Ghara *et al.*, and Roy *et al.* where they suggested a long-range magnetic ordering of $\mathrm{CoAl_2O_4}$ with inversion parameter $x \sim 0.05$ [20,26]. To readily compare the data, we have adopted polycrystalline data with site disorder $\sim$0.05 from Ref. [26]. We see that the single crystalline data has a sharper peak shape with nearly 1 K higher ordering temperature, which indicates that our sample has site disorder less than 0.05. To estimate the magnetic contribution [$C_{\rm Mag}(T)$] from the total heat capacity, the phonon contribution is calculated using a combined Debye-Einstein model as given by the following equation:

$$C_{\rm ph} = C_{\rm Debye} + C_{\rm Einstein} = \frac{9Ra_1}{x_D^3}\int_0^{x_D}\frac{x^4 e^x}{(e^x-1)^2}dx + 3R\sum_{n=1}^{2} b_n \frac{x_{E,n}^2 e^{x_{E,n}}}{(e^{x_{E,n}}-1)^2},$$

Where R is the universal gas constant, $x_{D,E} = \theta_{D,E}/T$, and $\theta_{D,E}$ is the Debye and Einstein temperatures, respectively. The C_P data in the range of 50–100 K has been fitted with the above equation and shown in Fig. 4(a). One Debye and two Einstein terms have been used for the fit. In the Debye-Einstein model, the total number of modes is equal to the number of atoms in the formula unit, and the used coefficients of Debye and Einstein contributions a_1, b_1, and b_2 are 1, 1, and 5, respectively [26].

The fitting was entirely satisfactory, and the fitted value was extrapolated down to the low temperature. The magnetic contribution was then calculated by subtracting the phonon contributions from the overall measured sample heat capacity and shown in Fig. 4(b). For an easier comparison of our data, we have also included the polycrystalline data adopted from Ref. [26]. We can see a slightly higher value of magnetic contribution than the previously reported value for the $\mathrm{CoAl_2O_4}$ compound with $\sim$0.05 site inversion [26]. As we know that the magnetic contribution reduces with the increasing disorder, we argue that our single-crystal sample may have an inversion degree slightly smaller than 0.05, which could not be derived precisely from the x-ray data refinement. As calculated from the following equation, the magnetic contribution associated entropy is shown in the inset of Fig. 4(b), which is in good agreement with the inversion parameter $\leqslant$0.05 [26]. For comparison, we have again incorporated the polycrystalline

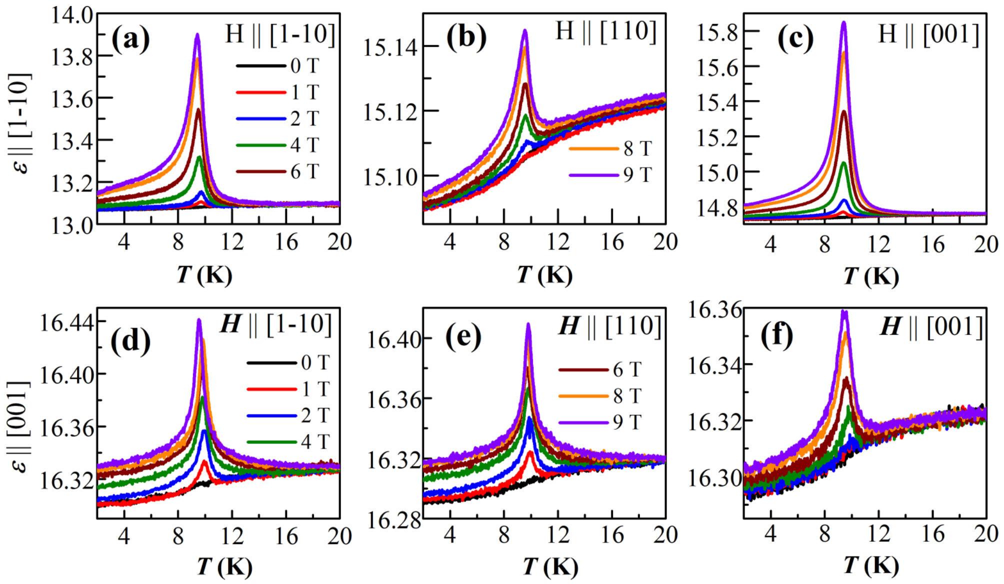

FIG. 5. Dielectric constant behavior as a function of temperature measured at 100 kHz along the [1–10] (upper panel) and [001] (lower panel) directions under magnetic fields along [1–10] (a), (d), [110] (b), (e), and [001] (c), (f).

data taken from Ref. [26]. We see that our single crystal has higher magnetic entropy than the polycrystalline sample with disorder 0.05. Since the Co^{2+} ions in the tetrahedral site are in high spin state configuration, the magnetic entropy should be $R\ln(2S+1) = R\ln 4 = 11.5\,\mathrm{J/mol\,K}$. Our experimental value ($\sim$ 9 J/mol K) indicates that there can be a finite amount of site disorder of Co^{2+} and Al^{3+} responsible for the discrepancy.

$$\Delta S_{\mathrm{Mag}}(T) = \int_0^T \frac{C_{\mathrm{Mag}}(T)}{T}\,dT$$

C. Magnetodielectric effect

Temperature dependence of dielectric constant (ε_r) is measured at 100 kHz in the range of 2 – 30 K along the [1–10] and [001] directions while applying various magnetic fields (0, 1, 2, 4, 6, 8, and 9 T) along [1–10], [110], and [001]. At $\mu_0 H = 0\,\mathrm{T}$ (where μ_0 is the magnetic permeability of vacuum), ε_r shows only a broad step near the magnetic ordering [Fig. 5(b)]. By applying a magnetic field, ε_r shows a λ-shaped peak near the magnetization peak around 10 K along all the measured directions. However, the intensities and widths of the peaks are quite different, along various directions of measurements and the applied magnetic field's various directions. The peak has the highest intensity along [1–10] when the magnetic field is applied along the [001] direction [Fig. 5(c)] ($\Delta\varepsilon_r(9T) \sim 0.8$). On the other hand, the enhancement of the peak is less intense under applied field along [110] [Fig. 5(b)] ($\Delta\varepsilon_r(9T) \sim 0.03$).

Further, the dielectric constant anomaly along [001] has a comparatively lower intensity for all the directions of the applied magnetic field [Fig. 5(d)–5(f)]. All these results confirm an intrinsic magnetodielectric effect with a significant anisotropy. The dielectric peak, which appears only under the applied magnetic field, confirms a magnetoelectric transition present in $\mathrm{CoAl_2O_4}$, which agrees with the earlier report in polycrystalline $\mathrm{CoAl_2O_4}$ [26]. The magnetodielectric effect [$\Delta\varepsilon = [\varepsilon(H) - \varepsilon(0)]/\varepsilon(0)$] measured along [110] direction under magnetic field along [110] and [001] directions is shown in Fig. 6.

A remarkable magnetodielectric effect can be noticed along the [110] direction for both the magnetic field directions, e.g., ~35% for [001] and ~12% for [110] direction at the 9-T field near the transition temperatures. A temperature dependent dielectric constant behavior along the [110] direction is given in the Supplemental Material [28]. It is worth mentioning that this type of magnetic field induced a peak in ε, and magnetocapacitance was observed in $\mathrm{Cr_2O_3}$ at the magnetoelectric transition temperature. Therefore, these results indicate a possible magnetoelectric effect in this sample.

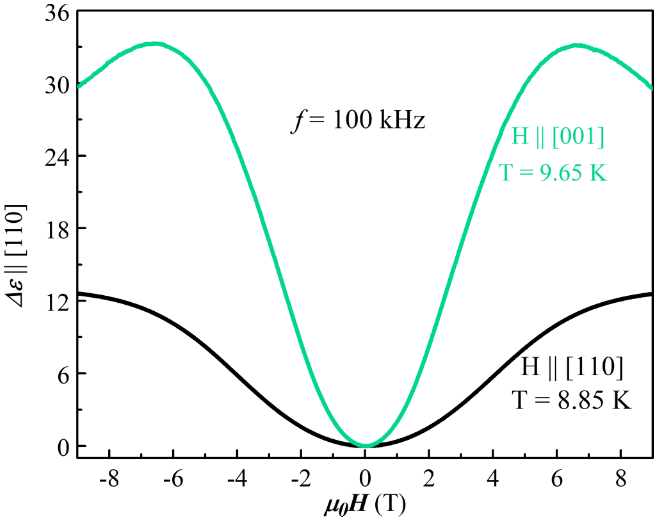

FIG. 6. Magnetodielectric effect along [110] direction under magnetic field along [110] and [001].

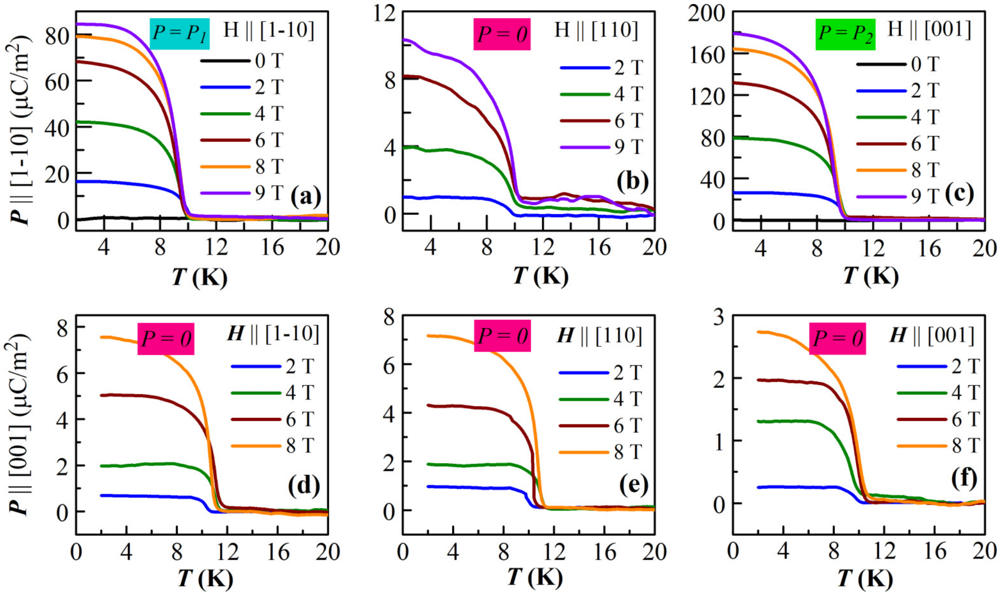

FIG. 7. Polarization behavior in $CoAl_2O_4$ single crystal obtained through integrating the measured pyrocurrent over the time along [1–10] and [001] directions during applied various magnetic fields along the [1–10], [110], and [001] directions.

D. Magnetoelectric effect

Pyrocurrent was recorded along all various directions under various applied magnetic fields as performed in the dielectric measurements. To observe the magnetoelectric polarization in the pyrocurrent measurements, the sample was first poled across the magnetic transition (from 30 to 2 K) with an electric field of 10 kV/cm and various magnetic fields. At 2 K, the electric field was removed, and the current was recorded while warming the sample from 2 to 20 K in the presence of a magnetic field. Figures 7(a)–7(f) show T dependence of integrated current over the time, i.e., polarization (P) along the [1–10] and [001] with H along the [1–10], [110], and [001] directions. Although no polarization is observed along any direction at 0 T, the P arises below the dielectric anomaly temperature by applying H along all the directions. This confirms the magnetoelectric effect in the sample. It is to be noted that the electric polarization in our single-crystalline $CoAl_2O_4$ is almost ten times higher than the observed polarization in polycrystalline $CoAl_2O_4$ with the disorder $\sim$0.05 [26]. Thus, the ten times higher polarization can be due to both the single-crystal nature of the sample and the lower inversion degree present in our sample, as evidenced by our heat capacity data. It is essential to notice that the polarization values are different along various measured directions and magnetic field directions. The significant polarization is observed along [1–10] under H along [1–10], denoted as P_1 and H along [001], denoted as P_2.

The polarization along [1–10] under the magnetic field along [110] is very small compared to the maximum observed polarization, which is in accordance with the magnetoelectric (ME) interaction (see below) that suggests the absence of electric polarization in this geometry. Therefore, the small experimentally observed value [Fig. 7(b)] can be regarded as a slight misalignment of the crystal or magnetic field directions, and we consider it a zero-polarization state, i.e., $P = 0$. Similarly, the polarization along [001] was negligible for all the magnetic field directions [Figs. 7(d)–7(f)] following the ME interactions. These results are in good agreement with the dielectric data, where we observed a similar intensity of the dielectric peaks [Figs. 5(a)–5(f)]. The induced P is almost linear with the magnetic field for all magnetic field directions, which confirms the material's linear magnetoelectric effect. The linear magnetoelectric coefficient was calculated from the slope of the linear fit of the P versus H data for P along [1–10] under H along [001] as shown in Fig. 8, which is found to be 27.3 ps/m, one order of magnitude higher than that observed in polycrystalline $CoAl_2O_4$ [26].

Since the observed linear magnetoelectric is not compatible with the spiral spin liquid state, we consider the magnetic ground state as a long-range antiferromagnetically

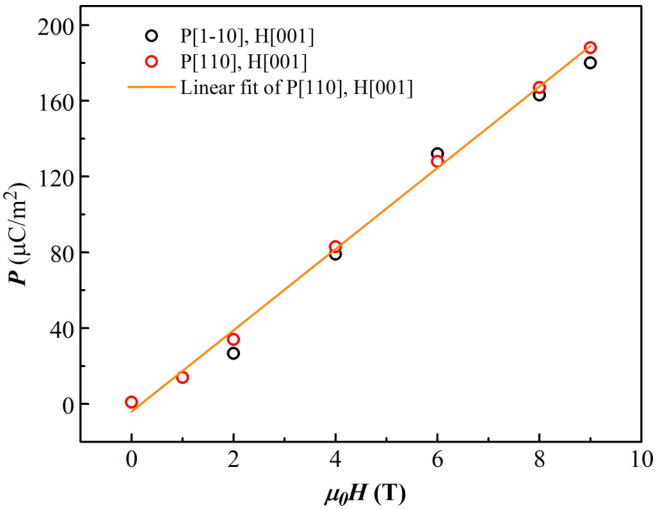

FIG. 8. Polarization versus magnetic field data at 2 K along the [1–10] (black circles) and [110] (red circles) directions along with the linear fit (orange line).

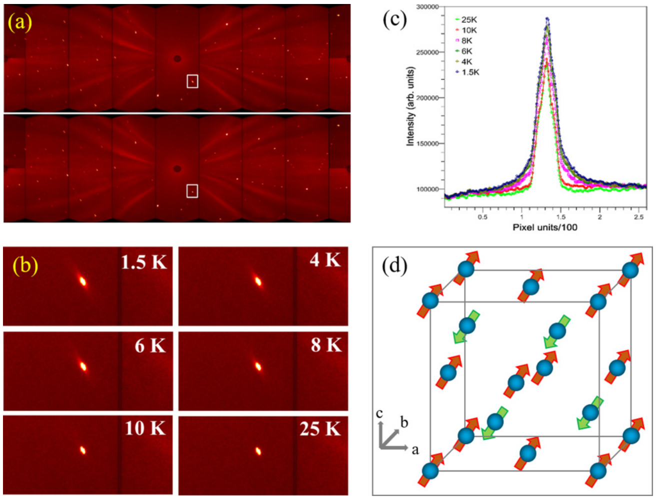

FIG. 9. (a) Comparative Laue diffraction pattern at 1.5 K (top) and 25 K (bottom). The white box showing [−200] reflection. (b) Temperature evolution of the [−200] reflection. (c) The integrated intensity of the [−200] reflection along [100] as a function of temperature. (d) AFM spin structure below T_N as proposed from the neutron and theoretical model.

ordered state [26]. Although the magnetic properties are isotropic, the electrical polarization and dielectric constant are highly anisotropic, further confirming the long-range magnetic ground state. As reported in Co_3O_4, the magnetic point group would be either $I4_1'/a'm'd$ or $R\bar{3}'m'$ where both of them allow the magnetoelectric effect. Therefore, for a detailed microscopic picture, a neutron diffraction experiment is necessary.

E. Neutron Laue diffraction

We have looked at the Laue diffraction pattern using the neutron beamline CYCLOPS at ILL to get more information about the magnetic ordering. A comparative Laue pattern of the 1.5 K (top) and 25 K (bottom) is shown in Fig. 9(a) where the [−200] reflections have been highlighted with a white square. We see an increased intensity in this reflection below the magnetic ordering temperature. The selected reflection's temperature evolution corresponds to the [−200] peak is shown in Fig. 9(b). Based on the Laue diffraction, the propagation vector is $\mathbf{k} = (0, 0, 0)$, as no new reflections are observed between the paramagnetic (25 K) and the ordered phases (1.5 K). Moreover, the increase of intensity below the ordering temperature suggests the occurrence of long-range magnetic order, which is in agreement with the powder neutron diffraction study by Roy *et al.* [20]. The previous single-crystal study suggested a spiral-spin-liquid state in which the sample has nearly 8% site inversion with a magnetic ordering temperature of ∼8 K [18]. Another single-crystal study suggested a kinetically inhibited long-range ordering due to domain wall freezing where the crystal underwent a first-order transition at ∼ 6 K [22]. Hence, we argue that the site intermixing plays a crucial role in the variety of features in this spinel compound.

We have also presented the intensity of the [−200] reflection, including the primary reflection and the diffuse scattering, which is extended along the [001] direction [Fig. 9(c)]. The x coordinates represent the position, i.e., basically pixels. The green and red curves, 25 and 10 K respectively, correspond to the paramagnetic phase. Neither of these curves presents any signal of diffuse scattering. However, we can see the robust and diffusive nature in the peaks below the magnetic ordering; thus, the observed Lorentzian contribution to the tails of the [−200] reflection should have a magnetic origin. The elongation of the diffuse scattering is along the [001] direction, and therefore the magnetic contribution at the origin of this signal should be contained in the *ab* plane. The difference observed between the magnetization curves measured at different orientations [see Fig. 3(a)] can be explained based on the AFM model and short-range magnetic order (or a spin-liquid behavior) in the *ab* plane due to the non-negligible frustration is this system. When the magnetic field is applied along the *ab* plane, the magnetic moments contained in the *ab* plane, and responsible for the diffuse scattering, are more easily polarized along the direction of the magnetic field, and therefore an increase of magnetization is expected, as is observed in Fig. 3(a). Finally, below 10 K, the intensity of the [−200] reflection increases with decreasing temperature, suggesting a commensurate $\mathbf{k} = 0$ magnetic structure. Further investigations are required to understand the nature of magnetic ordering since the cationic inversion strongly influences the magnetic properties.

F. Easy axis determination from electric polarization

The cubic symmetry of $CoAl_2O_4$ suggests two most probable easy magnetic axis directions, i.e., either along [001] or along [111]. From the ratio of polarizations determined in different measurement geometries, one can find the easy magnetic axis. As found earlier, the magnetoelectric effect in A-site AFM spinel is due to a single-ion contribution [16,29]. According to the tetrahedral local symmetry at the Co sites, the local spin-dependent electric dipole moments $\vec{d}_1$ and $\vec{d}_2$ of the two Co sites in the primitive unit cell with spins $\vec{S}_1$ and $\vec{S}_2$ can be written as

$$\vec{d}_1 = c(S_{1y}S_{1z}, S_{1x}S_{1z}, S_{1x}S_{1y}),$$

$$\vec{d}_2 = -c(S_{2y}S_{2z}, S_{2x}S_{2z}, S_{2x}S_{2y}),$$

where c is a constant. Introducing the AFM $\vec{L} = \vec{S}_2 - \vec{S}_1$ and ferromagnetic $\vec{M} = \vec{S}_1 + \vec{S}_2$ order parameters, one can find the electric polarization $\vec{P} \sim (\vec{d}_1 + \vec{d}_2)$ as $\vec{P} \sim (L_zM_y + L_yM_z, L_zM_x + L_xM_z, L_yM_x + L_xM_y)$, which follows the phenomenological magnetoelectric interaction [16,29]. $P||[1–10]$ at $H||[001]$ was considered as P_2, which is almost the same as $P||[110]$ at $H||[001]$ as expected from the $Fd\bar{3}m$ symmetry [29]. $P||[1–10]$ at $H||[1–10]$ was considered as P_1. For the case of $P||[001]$, the polarization should vanish for all studied magnetic field directions, and we observe a very small polarization, which can be due to slight misalignment of the crystal or the applied magnetic field directions. Assuming $P = P_1$ and P_2 for $P||[1–10]$ at $H||[1–10]$ and $H||[001]$, respectively, we have calculated their ratio of P_1/P_2. Using the above equations, one can show that for the easy axis along [111] and magnetic fields higher than the spin-flop value,

P_1/P_2 should be equal to $\mathbf{1/\sqrt{3}}$ [16]. On the other hand, if the easy axis is along [001], the P_1/P_2 ratio should be equal to $\sqrt{\mathbf{2}}$. We observed a spin flop transition from our polarization and magnetization data, and the P_1/P_2 ratio is close to $\mathbf{1/\sqrt{3}}$. Since the magnetic anisotropy in $CoAl_2O_4$ is quite low, and the AFM vector can easily orient perpendicular to the magnetic field, the value $1/\sqrt{3} \approx 0.58$ is quite close to that observed for $P||[1–10]$. Therefore, we suggest that the easy axis should be along the [111] direction. If the easy axis was along [001], then $P||[1–10]$ at $H||[1–10]$ should be bigger than at $H||[001]$, which is not the case. We would like to point out here that a previous neutron diffraction experiment in the powder sample proposed a collinear magnetic state with easy axis along [001] direction similar to the Co_3O_4 magnetic structure [20]. In contrast, we determine the easy magnetic axis to be along [111] and the magnetic point group $R\bar{3}'m'$, similar to the case of $MnGa_2O_4$, which has the easy magnetic axis along [111] as demonstrated in Fig. 9(d) [16]. However, a further detailed investigation of the magnetic structure including magnetic domains are necessary to understand the complicated scenario in this frustrated magnetic spinel, which can also account the magnetoelectric behavior in the frustrated system.

IV. CONCLUSION

In conclusion, we have grown $CoAl_2O_4$ single crystal with minimum site disorder, which indicated long-range AFM behavior in the magnetization and heat capacity. Moreover, the increase of intensity on top of the nuclear reflections observed in the Laue patterns confirms a commensurate long-range magnetic order with $\mathbf{k} = 0$. This long-range order coexists with a non-negligible short-range contribution mainly contained in the *ab* plane, as having been determined from the occurrence of Lorentzian tails along the [001] direction around the magnetic reflection bellow T_N. Electric polarization is observed below the magnetic ordering under the magnetic field, depending on the crystallographic directions and applied magnetic field directions. The linear magnetoelectric coefficient in the $P||[110]$ and $H||[001]$ geometry reaches 27.3 ps/m. Based on the magnetoelectric measurements in various geometries, we determine the magnetic easy to be along the [111] direction resulting in $R\bar{3}'m'$ magnetic symmetry. Thus, this study contributes to understanding of the magnetic ground state in the A-site magnetic spinel $CoAl_2O_4$.

ACKNOWLEDGMENTS

N.V.T.-O. acknowledges financial support from the Russian Foundation for Basic Research Grant No. 18-52-80028 (BRICS STI Framework Programme). A.S. thank the International Center for Materials Science (ICMS) and Sheikh Saqr Laboratory (SSL) for various experimental facilities. A.S. also acknowledges BRICS research project, Department of Science and Technology, Government of India, for a research grant [Sl. No. DST/IMRCD/BRICS/PilotCall2/EMPMM/2018(g)].

[1] D. Bergman, J. Alicea, E. Gull, S. Trebst, and L. Balents, Nat. Phys. **3**, 487 (2007).

[2] J.-S. Bernier, M. J. Lawler, and Y. B. Kim, Phys. Rev. Lett. **101**, 047201 (2008).

[3] A. P. Ramirez, A. Hayashi, R. A. Cava, R. Siddharthan, and B. Shastry, Nature (London) **399**, 333 (1999).

[4] S. T. Bramwell and M. J. Gingras, Science **294**, 1495 (2001).

[5] S. Kondo, D. C. Johnston, C. A. Swenson, F. Borsa, A. V. Mahajan, L. L. Miller, T. Gu, A. I. Goldman, M. B. Maple, D. Gajewski, E. J Freeman, N. R. Dilley, R. P Dickey, J. K. Merrin, K. Kojima, G. M. Luke, Y. M. Uemura, O. Chmaissem, and J. D. Jorgensen, Phys. Rev. Lett. **78**, 3729 (1997).

[6] F. L. Buessen, M. Hering, J. Reuther, and S. Trebst, Phys. Rev. Lett. **120**, 057201 (2018).

[7] J. Oitmaa, Phys. Rev. B **99**, 134407 (2019).

[8] W. Roth, J. Phys. **25**, 507 (1964).

[9] R. Fichtl, V. Tsurkan, P. Lunkenheimer, J. Hemberger, V. Fritsch, H.-A. Krug von Nidda, E.-W. Scheidt, and A. Loidl, Phys. Rev. Lett. **94**, 027601 (2005).

[10] S. Das, D. Nafday, T. Saha-Dasgupta, and A. Paramekanti, Phys. Rev. B **100**, 140408(R) (2019).

[11] Y. Iqbal, T. Müller, H.O. Jeschke, R. Thomale, and J. Reuther, Phys. Rev. B **98**, 064427 (2018).

[12] S. Gao, O. Zaharko, V. Tsurkan, Y. Su, J. S. White, G. S. Tucker, B. Roessli, F. Bourdarot, R. Sibille, and D. Chernyshov, Nat. Phys. **13**, 157 (2017).

[13] S. Gao, H. D. Rosales, F. A. G. Albarracín, V. Tsurkan, G. Kaur, T. Fennell, P. Steffens, M. Boehm, P. Čermák, and A. Schneidewind, Nature (London) **586**, 37 (2020).

[14] N. Tristan, J. Hemberger, A. Krimmel, H. A. Krug von Nidda, V. Tsurkan, and A. Loidl, Phys. Rev. B **72**, 174404 (2005).

[15] H. Cho, R. Nirmala, J. Jeong, P. J. Baker, H. Takeda, N. Mera, S. J. Blundell, M. Takigawa, D. T. Adroja, and J.-G. Park, Phys. Rev. B **102**, 014439 (2020).

[16] R. Saha, S. Ghara, E. Suard, D. H. Jang, K. H. Kim, N. V. Ter-Oganessian, and A. Sundaresan, Phys. Rev. B **94**, 014428 (2016).

[17] T. Suzuki, H. Nagai, M. Nohara, and H. Takagi, J. Phys. Condens. Matter **19**, 145265 (2007).

[18] O. Zaharko, N. B. Christensen, A. Cervellino, V. Tsurkan, A. Maljuk, U. Stuhr, C. Niedermayer, F. Yokaichiya, D. Argyriou, M. Boehm, and A. Loidl, Phys. Rev. B **84**, 094403 (2011).

[19] K. Hanashima, Y. Kodama, D. Akahoshi, C. Kanadani, and T. Saito, J. Phys. Soc. Jpn. **82**, 024702 (2013).

[20] B. Roy, A. Pandey, Q. Zhang, T. Heitmann, D. Vaknin, D. C. Johnston, and Y. Furukawa, Phys. Rev. B **88**, 174415 (2013).

[21] O. Zaharko, S. Tóth, O. Sendetskyi, A. Cervellino, A. Wolter-Giraud, T. Dey, A. Maljuk, and V. Tsurkan, Phys. Rev. B **90**, 134416 (2014).

[22] G. J. MacDougall, D. Gout, J. L. Zarestky, G. Ehlers, A. Podlesnyak, M. A. McGuire, D. Mandrus, and S. E. Nagler, Proc. Natl. Acad. Sci. USA **108**, 15693 (2011).

[23] M. Iakovleva, E. Vavilova, H.-J. Grafe, S. Zimmermann, A. Alfonsov, H. Luetkens, H.-H. Klauss, A. Maljuk, S. Wurmehl, B. Büchner, and V. Kataev, Phys. Rev. B **91**, 144419 (2015).

[24] G. J. MacDougall, A. A. Aczel, Y. Su, W. Schweika, E. Faulhaber, A. Schneidewind, A. D. Christianson, J. L. Zarestky,

H. Zhou, D. Mandrus, and S. E. Nagler, Phys. Rev. B **94**, 184422 (2016).

[25] T. Naka, H. Mamiya, K. Takehana, N. Tsujii, Y. Imanaka, S. Ishii, T. Nakane, M. Nakayama, and T. Uchikoshi, arXiv:1811.00186 (2018).

[26] S. Ghara, N. V. Ter-Oganessian, and A. Sundaresan, Phys. Rev. B **95**, 094404 (2017).

[27] A. Maljuk, V. Tsurkan, V. Zestrea, O. Zaharko, A. Cervellino, A. Loidl, and D. Argyriou, J. Cryst. Growth. **311**, 3997 (2009).

[28] See Supplemental Material at http://link.aps.org/supplemental/10.1103/PhysRevB.103.094406 for x-ray diffraction refinement parameter details, linear fit of magnetic susceptibility, detailed magnetization, and dielectric data.

[29] N. Ter-Oganessian, J. Magn. Magn. Mater. **364**, 47 (2014).